Hindawi
Journal of Healthcare Engineering
Volume 2023, Article ID 9825050, 1 page
https://doi.org/10.1155/2023/9825050

Retraction

Retracted: Role of CT Images in the Diagnosis of Common Acute Abdominal Diseases in General Surgery

Journal of Healthcare Engineering

Received 10 October 2023; Accepted 10 October 2023; Published 11 October 2023

This article has been retracted by Hindawi following an investigation undertaken by the publisher [1]. This investigation has uncovered evidence of one or more of the following indicators of systematic manipulation of the publication process:

(1) Discrepancies in scope
(2) Discrepancies in the description of the research reported
(3) Discrepancies between the availability of data and the research described
(4) Inappropriate citations
(5) Incoherent, meaningless and/or irrelevant content included in the article
(6) Peer-review manipulation

The presence of these indicators undermines our confidence in the integrity of the article's content and we cannot, therefore, vouch for its reliability. Please note that this notice is intended solely to alert readers that the content of this article is unreliable. We have not investigated whether authors were aware of or involved in the systematic manipulation of the publication process.

In addition, our investigation has also shown that one or more of the following human-subject reporting requirements has not been met in this article: ethical approval by an Institutional Review Board (IRB) committee or equivalent, patient/participant consent to participate, and/or agreement to publish patient/participant details (where relevant).

Wiley and Hindawi regrets that the usual quality checks did not identify these issues before publication and have since put additional measures in place to safeguard research integrity.

We wish to credit our own Research Integrity and Research Publishing teams and anonymous and named external researchers and research integrity experts for contributing to this investigation.

The corresponding author, as the representative of all authors, has been given the opportunity to register their agreement or disagreement to this retraction. We have kept a record of any response received.

References

[1] Y. Nan, Z. Zhang, J. Zhang, B. Jiang, Y. Zhu, and L. Zhang, "Role of CT Images in the Diagnosis of Common Acute Abdominal Diseases in General Surgery," *Journal of Healthcare Engineering*, vol. 2022, Article ID 5732357, 13 pages, 2022.

Hindawi
Journal of Healthcare Engineering
Volume 2022, Article ID 5732357, 13 pages
https://doi.org/10.1155/2022/5732357

Research Article

Role of CT Images in the Diagnosis of Common Acute Abdominal Diseases in General Surgery

Yunguang Nan,[1] Zuyan Zhang,[2] Jianbo Zhang,[1] Bo Jiang,[1] Yuxi Zhu ,[1] and Li Zhang [2]

[1]*General Surgery, Shuyang Benevolent Hospital, Suqian 223600, Jiangsu, China*
[2]*Imaging Department, Shuyang Benevolent Hospital, Suqian 223600, Jiangsu, China*

Correspondence should be addressed to Yuxi Zhu; 345419092@qq.com and Li Zhang; 161841356@masu.edu.cn

Received 8 December 2021; Accepted 16 January 2022; Published 23 March 2022

Academic Editor: Alireza Souri

Acute abdomen is a clinical emergency disease with acute abdominal pain as the main prominent feature. Through severe disease changes in intra-abdominal, extrapelvic, and retroperitoneal tissues and organs, symptoms and clinical signs led by abdominal pain are formed. This article mainly explores the role of CT imaging diagnosis in common acute abdominal diseases in general surgery. In this paper, the use of computer-aided CT scan imaging technology in pulmonary nodules was firstly investigated, and the image segmentation algorithms based on CT images were given, including the spatial domain fuzzy C-mean clustering separation algorithm and the spatial domain fuzzy clustering level set semiautomatic separation algorithm, then the treatment of acute abdomen under the concept of ERAS was explored, and the treatment of ERAS under CT images of the acute abdomen was analyzed and studied. The empirical research results show that the ERAS's concept is guided by the undergoing national nutritional support with the traditional perioperative management. Compared to 12.9% of complications in traditional CPM groups, the recall rate of complications after ERAS group was only 6.01%, the improvement was obvious and the results were statistically significant ($P < 0.05$). Postoperative hospitalization time was also 4.62 days from 7.93 days, thus controlling the clinical risks of perioperative periods, providing a benefit to patient life.

1. Introduction

Surgical emergencies often require emergency surgery, and clinicians tend to focus on saving patients' lives, while often neglecting to anticipate the disturbance of patients' internal environment, intraoperative damage control, postoperative recovery, and their own feelings during the perioperative period. The introduction of the FTS concept has fundamentally changed the clinicians' way of thinking. It requires the clinician to pay attention to the patient's preoperative psychological and physiological status, avoid unnecessary invasive operations to reduce various stress reactions, pay attention to intraoperative warming and control the amount of rehydration to facilitate the recovery of various physiological functions after surgery, and require the patient to eat and get out of bed as early as possible after surgery to prevent various complications. All these are aimed at making the patients' perioperative physiological functions close to or return to the normal level as soon as possible, reducing pain and restoring health as soon as possible.

With the continuous development of computer application technology, computer-aided CT imaging technology has been widely used in the medical industry, and CT imaging technology uses digital image processing technology to analyze medical image processing data in order to obtain auxiliary signals that are of practical use to physicians in clinical treatment. As with traditional medical examinations, the use of CT imaging technology in clinical applications will reduce the pressure on physicians to read films, improve the accuracy and effectiveness of treatment, and reduce inconsistencies in treatment conclusions due to physician experience and knowledge levels during treatment; in the long run, the use of computer-aided creation of CT imaging products is of great significance in improving current medical technology.

According to the research progress at home and abroad, different scholars also have some collaborative research in

CT imaging diagnosis: Zhang S used the classical LeNet-5 model to classify pulmonary nodules in chest CT images, including benign and malignant pulmonary nodules, and different degrees of malignancy of malignant nodules. A 10-folder cross-validation (CV) was also implemented to demonstrate the robustness of the training classification model. The results showed that LeNet-5 migration learning was effective in classifying lung nodules from chest CT images, with mean Top-1 accuracy rates of 97.041% and 96.685%, respectively [1]. The objectives of the Li Y study were to determine the rate of radiologist misdiagnosis of coronavirus disease (COVID-19) in 2019 and assess the performance of chest CT in the diagnosis and management of COVID-19. CT features of COVID-19 are reported and compared with those of other viruses to familiarize radiologists with possible CT patterns. The results of the study found that chest CT had a low rate of missed diagnosis of COVID-19 (3.9%, 2/51) and could be used as a standard method for rapid diagnosis of COVID-19 to optimize patient management. However, CT is still limited in identifying specific viruses and differentiating them [2]. Metintas et al. aim to compare the diagnostic yield and safety of CT scan-guided pleural biopsy using an Abrams needle (CT-ANPB) with ultrasound-assisted pleural biopsy using a cutting needle (US–CNPB). For patients with CT scans showing pleural effusion and associated pleural thickening, the preferred diagnostic intervention is CT-ANPB, and US-CNPB should be used primarily in cases where only pleural thickening but not pleural effusion is found [3]. Ropelle et al. summarize that the hypothalamus is a brain region that collects information about the nutritional status of the body and controls the release of multiple metabolic signaling molecules (e.g., insulin and leptin) to maintain homeostasis in the body. Studies have shown that physical activity reorganizes the set point of nutritional homeostasis through anti-inflammatory signaling mediated by interleukin (IL)-6 and IL-10 in the rodent hypothalamus. Thus, IL-6 and IL-10 are important physiological factors in exercise-mediated central insulin and leptin actions, linking them to hypothalamic endoplasmic reticulum stress and inflammation [4, 5]. Dijk et al. investigated improved prediction of XER12m and STIC12m with patient-specific features based on CT image biomarkers (IBM). The prediction of XER12m could be significantly improved by adding the IBM "ShortRunEmphasis" (SRE), which quantifies parotid tissue heterogeneity, to a model with mean contralateral parotid dose and XERbase [6]. Dong et al. propose an averaging image-induced nonlocal mean (aviNLM) filter for each energy-specific image recovery. The proposed aviNLM algorithm produces recovery results by performing a nonlocal weighted averaging operation for noise-energy specific images, where there is a nonlocal weight matrix between the target and prior images. Experimental results show that the current aviNLM algorithm has the potential to reduce radiation dose by reducing mAs in SCT imaging, and it may be useful for some other clinical applications, such as in myocardial perfusion imaging and radiotherapy [7]. The Hao et al. study aimed to transform the edge-preserving region noise smoothing paradigm into a texture-preserving framework for LdCT image reconstruction, while preserving the advantages of the MRF neighborhood system in edge preservation. To demonstrate the feasibility of the proposed reconstruction framework, experiments using clinical patient scans were performed. The experimental results showed that significant gains were obtained from the a priori knowledge of LdCT image reconstruction using the commonly used Haralick texture measurements. Therefore, it is hypothesized that texture-preserving LdCT reconstruction is superior to the edge-preserving region smoothing paradigm in texture-specific clinical applications [8, 9]. Helma et al. explored the efficiencies of data mining and machine learning algorithms induced by mutant moiety (SAR) from nonmutated data concentration. From the application's machine learning technology, the rule learner Part and support vector machines give the best results, although the difference between the learning algorithms is small [10]. However, these scholars did not explore the role of common acute abdominal conditions in general surgery in conjunction with diagnostic CT imaging.

The innovation of this paper is reflected in discussing the application of computer-aided CT scan images in pulmonary nodules and proposing an image segmentation algorithm based on CT images and then exploring the treatment of acute abdomen under the concept of ERAS and analyzing the study of ERAS for acute abdomen under CT images.

2. Experimental Methods for the Diagnosis of Common Acute Abdominal Diseases in General Surgery Based on CT Images

2.1. Application of Computer-Aided CT Scan Images in Lung Nodules. For a long time, the interpretation of medical pictures has been performed by radiologists, and experienced physicians can determine whether a suspicious shadow is benign or malignant by examining the grayscale value, size, margin, location, and other signal characteristics of the suspicious shadow in medical pictures, but usually an in-depth puncture is required to extract a small number of biopsies for pathological analysis before a final diagnosis can be made. However, physicians' understanding of medical images is influenced by many factors, including the complexity of the imaging mechanism of medical images and the differences in the performance of various medical imaging devices, which inevitably lead to conditions such as large individual differences, blurred boundaries, and prominent noise and artifacts in the resulting images [11]. Moreover, the pathology of pulmonary nodule formation is unclear, the lesion characteristics are diverse, and the clinical examination lacks specific norms, which makes the examination, identification, and classification of pulmonary nodules more difficult [12]. Therefore, making an accurate judgment based on a patient's image is sometimes not a simple task. The opinions of different doctors sometimes differ when examining the same image and are highly subjective [13]. At the same time, reading a large number of images is unbearable for physicians, who need to reduce the number of images read and the time spent on each image to make a

quick judgment, which can easily lead to misdiagnosis and missed cases [14]. Therefore, it is crucial to develop computer programs to help physicians read and analyze medical images through computer support.

However, for computer-assisted therapy, useful signals must be found in the images to make judgments. For example, Figure 1 shows the computer-aided CT image analysis [15]. Because of the partial volume effect and artifacts, there are often cases of different images of the same disease or even different diseases in the images, which causes great problems for computer-aided therapy [16]. While high-performance CAD systems often give medically accurate opinions, which in turn greatly improve the effectiveness and thus the accuracy of treatment, reduced-performance CAD systems not only often yield unsatisfactory results, but also increase the psychological burden on medical staff and even mislead them, thus achieving the opposite effect [17]. Although many research results have been obtained on CAD techniques for pulmonary nodules, and some CAD systems have been commercialized, these research results and application conditions are not perfect, or they are only effective for a certain type of suspected shadow, and their use is limited. Therefore, the current therapeutic efficacy of CAD systems does not yet meet the requirements of conventional medical imaging treatment for the characterization of benign and malignant pulmonary nodules [18].

Under the circumstances that the current CAD system cannot handle the diagnosis of pulmonary nodules, it is always advantageous to explore new solutions. The main purpose of this paper is to summarize the previous research results in various stages of lung nodule detection, and at the same time to try to design and develop a CAD system specifically for lung nodules with a new idea of lung nodule diagnosis, in order to expect to reduce the burden of medical personnel and to detect lung nodules more effectively [19]. Figure 2 shows the computer-assisted virtual drug screening process.

Lung cancer is extremely harmful to people's health. At present, the most effective way to deal with lung cancer is through regular lung CT scans, early detection of lung nodules, and timely diagnosis to improve survival rate [20]. A CAD system with high accuracy plays a pivotal role in reducing omissions or misdiagnosis by doctors and has important use value and practical significance.

2.2. Theories of Image Segmentation Algorithms Based on CT Images

2.2.1. Fuzzy C-Means Clustering Segmentation Algorithm in Spatial Domain. The fuzzy C-mean (FCM) clustering algorithm regards the pixels of the picture as a sample set and distinguishes the pixels of the picture according to the principles of similarity within the class and separation between classes [21]. FCM algorithm is the largest separation calculation used in fuzzy clustering calculation, and it is also commonly used in the field of medical vision image separation.

The typical FCM algorithm originated from K-means clustering calculation. After repeated iterations of the algorithm, all cost functions are simplified and clustered:

$$G = \sum_{a=1}^{K} \sum_{b==1}^{D} l_a - c_b^2. \tag{1}$$

The objective function of the FCM algorithm is

$$G = \sum_{a=1}^{K} \sum_{b==1}^{D} t_{ab}^h l_a - c_b^2, \tag{2}$$

where t_{ab} is a member function of the algorithm and must meet the following requirements:

$$\begin{gathered} \forall a, b, \sum_{b=1}^{D} t_{ab} = 1; \quad t_{ab} \in [0, 1], \\ \sum_{a=1}^{A} t_{ab} > 0. \end{gathered} \tag{3}$$

Member function t_{ab} and cluster center c_b can be solved iteratively according to the following formula until the objective function value is the smallest:

$$\begin{gathered} t_{ab} = \frac{l_a - c_b^{-2/(h-1)}}{\sum_{k==1}^{D} l_a - c_k^{-2/(h-1)}}, \\ c_b = \frac{\sum_{a=1}^{A} t_{ab}^h l_a}{\sum_{a=1}^{A} t_{ab}^h}. \end{gathered} \tag{4}$$

If the pixel characteristic value of an image is similar to the characteristic value of a cluster center level variable, then the image is given a higher fuzzy affiliation value; assuming that the difference between the image characteristic value and the characteristic value of a cluster center is large, then the image is given a lower fuzzy affiliation value [22]. The classic fuzzy C-means clustering algorithm can accurately separate the images initially, but the separation effect is not ideal for images with inconsistent gray levels and weak edge features.

The composition function operation method is described by the following formula:

$$t_{ab} = \frac{t_{ab}^m r_{ab}^n}{\sum_{k=1}^{D} t_{kb}^m r_{kb}^n}. \tag{5}$$

r_{ab}^n is the constructed spatial domain function including the membership degree of the neighboring pixels:

$$r_{ab}^n = \sum_{k \in A_a} t_{kb}. \tag{6}$$

In the clustering calculation, the expression of the spatial function method can be introduced into formula (4) and modified as a fuzzy membership degree.

2.2.2. Semiautomatic Segmentation Algorithm of Fuzzy Clustering Level Set in Spatial Domain. The FCM algorithm, after subdividing the graphical pixel point aggregation, uses

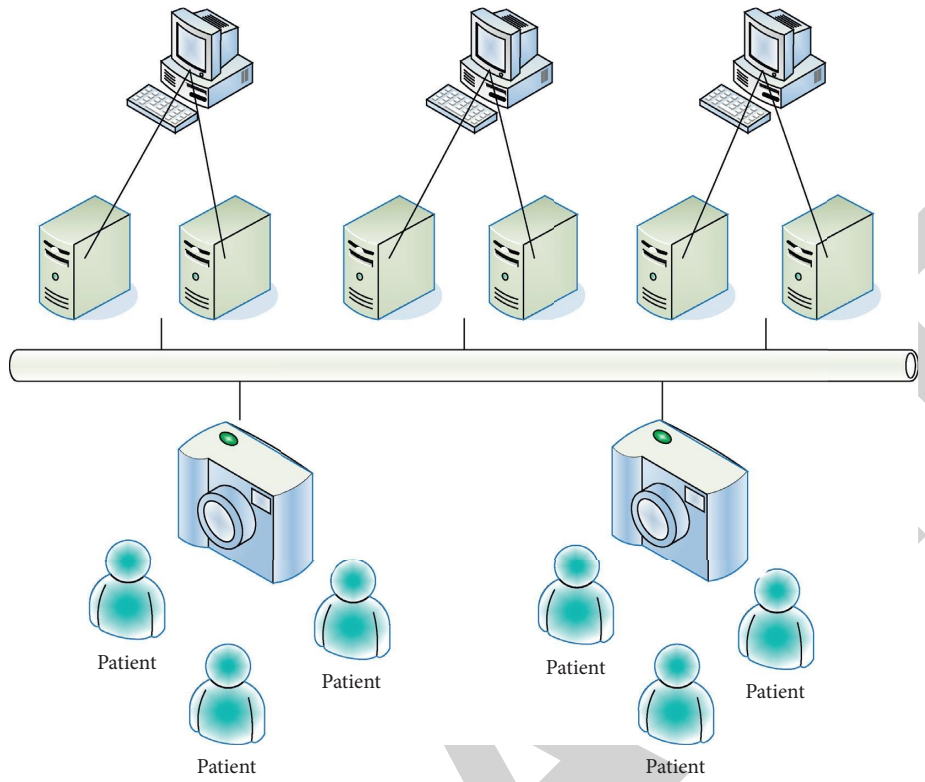

Figure 1: Computer-aided CT image analysis.

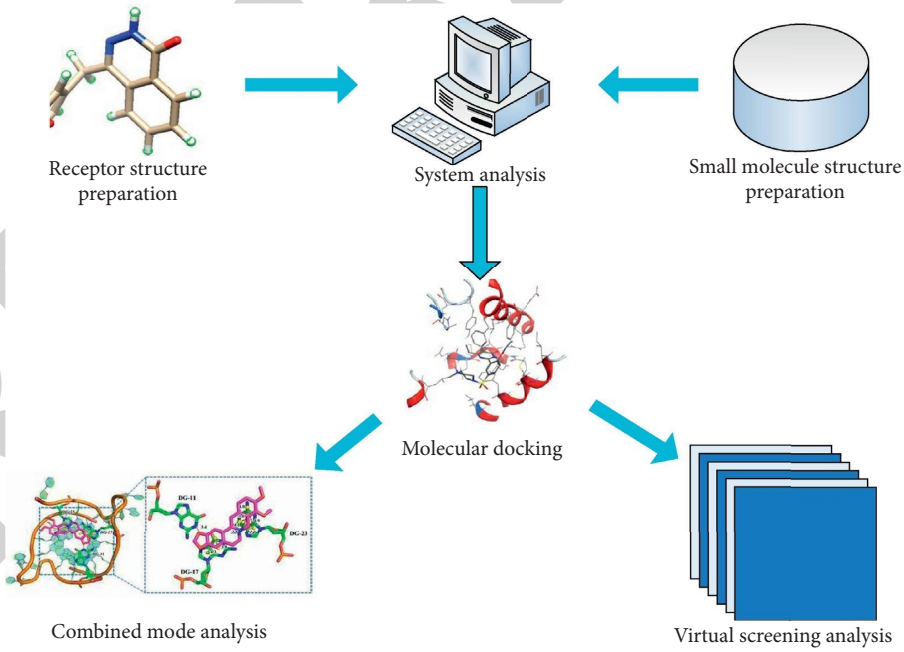

Figure 2: Computer-aided virtual drug screening.

the level set cutting operator to express a function in the highest one-dimensional space (called level set function) as a zero level set to cut the target contour shape and uses the curve evolution of the active contour model to cut the graph, as shown in Figure 3.

The traditional level set cut approach in the curve evolution step, for determining the sign of the level set function with the time distance function approach, must be periodically initialized, which leads to an excessive amount of statistics for the algorithm and unstable cut results

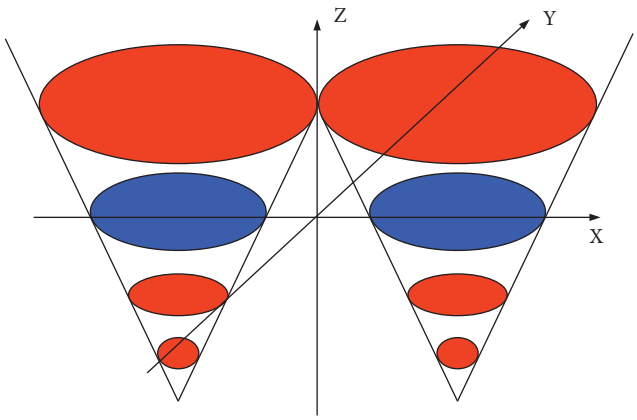

Figure 3: Schematic diagram of the evolution of the level set function.

[23, 24]. Moreover, the statistical time and quantization steps must also comply with the Courant–Friedrichs–Lewy (CFL) requirements, so the average value is usually taken to be smaller.

According to the above problems, you can choose a high-speed level set subdivision calculation that does not need to be initialized. The evolution formula of the level set algorithm is defined as

$$\frac{\partial \varphi}{\partial o} = t\gamma(\varphi) + \gamma(j, \varphi). \tag{7}$$

Here, φ is the signed distance function; $\gamma(\varphi)$ is the degree to which the level set function φ deviates from φ, and the expression is

$$\gamma(\varphi) = \triangle\varphi - \operatorname{div}\left(\frac{\nabla\varphi}{|\nabla\varphi|}\right), \tag{8}$$

where $\gamma(j, \varphi)$ is to guide the level set function to converge towards the boundary of the target of interest, and the expression is

$$\gamma(j, \varphi) = \rho\omega(\varphi)\operatorname{div}\left(\frac{\nabla\varphi}{|\nabla\varphi|}\right) + sj\omega(\varphi). \tag{9}$$

Here, ρ and s are constants. The expressions of $\omega(\varphi)$ and j are

$$\omega(a) = \begin{cases} \frac{1}{2\tau}\left[1 + \cos\frac{\pi a}{\tau}\right], & |a| \le \tau, \\ 0, & |a| \ge \tau, \end{cases} \qquad j = \frac{1}{1 + \left|\nabla\left(J_\alpha \otimes L\right)\right|^2}. \tag{10}$$

The level set algorithm initializes the level set function by establishing a region, instead of using the signed distance function to initialize it. Express the initialization function as

$$\varphi_0(a, b) = \begin{cases} -D, & \varphi_0(a, b) < 0, \\ D, & \text{otherwise}, \end{cases} \tag{11}$$

where D is a fixed constant.

The level set evolution formula adopts the finite difference method to discretize the calculation, and the obtained level set function iterative equation is

$$\varphi^{k+1}(a, b) = \varphi^k(a, b) + \beta\left[t\gamma\left(\varphi^k\right) + \gamma\left(j, \varphi^k\right)\right], \tag{12}$$

where β refers to the time step.

Both fuzzy C-mean clustering and level set separation calculations are very good image separation models and have been widely used in industrial image separation, but when the algorithms are applied to the field of medical image separation, each has limitations and is not widely adaptable [25]. The fuzzy clustering algorithm clusters the splitting objects for image pixel point similarity without affecting the spatial extent signal and boundary information of the image; while the horizontal set segmentation algorithm requires manual initialization, so the calculation of the splitting conclusion is not fixed, and for different types of horizontal separation objects, different types of parameters need to be set preferably, and if the parameters are chosen properly, the image separation effect is good, and on the contrary, the effect is not good [26].

Based on these problems, a level set calculation based on spatial domain fuzzy clustering is given to perform the segmentation of CT images of malignant cancers of the liver and kidney. The calculation first uses the spatial domain fuzzy C-mean clustering algorithm for the initial aggregation of image segmentation and then reinitializes the level set function based on the aggregation results.

The initial level set function is defined as

$$\varphi_0(a, b) = -4\tau(0.5 - E_k) \tag{13}$$

where τ is a parameter in the Dirac function and E_k is a binary image:

$$E_k = U_k \ge e_0, \quad e_0 \in (0, 1). \tag{14}$$

In the fuzzy level centralized split calculation, the parameter settings during the level set evolution will also affect the final split conclusion of the medical image. Therefore, for different types of medical images, the control parameter selection values need to be adjusted appropriately [27].

The parameters are automatically initialized according to the following formula:

$$\begin{cases} i = \int \omega(\varphi_0)\mathrm{d}a\mathrm{d}b, \\ \mu = \int H(\varphi_0)\mathrm{d}a\mathrm{d}b, \\ \aleph = \frac{\mu}{i}. \end{cases} \tag{15}$$

$H(\varphi_0)$ represents the Heaviside function, and the expression is

$$H(\varphi_0) = \begin{cases} 1, & \varphi \ge 0, \\ 0, & \varphi < 0, \end{cases} \qquad \begin{cases} t = \frac{0.2}{\aleph}, \\ \rho = \frac{0.1}{\aleph}. \end{cases} \tag{16}$$

The balloon force parameter is rewritten as follows:

$$J(E_k) = 1 - 2E_k. \tag{17}$$

The function term $\gamma(j, \varphi^k)$ in the level set evolution equation and iterative expression can be rewritten as

$$\gamma\left(j, \varphi^k\right) = \rho\,\omega(\varphi)\mathrm{div}\left(\frac{\nabla\varphi}{|\nabla\varphi|}\right) + J(E_k)j\omega(\varphi). \tag{18}$$

The level set segmentation calculation combined with the spatial domain fuzzy cluster analysis method fully considers the image space domain information, and the balloon force parameter covers the signal after the spatial domain fuzzy cluster analysis method, and the level set function can be initialized manually after the fuzzy cluster analysis method results, thus reducing the problem of unstable operation results caused by automatic initialization [28].

The basic idea of regional growth is to collect pixels with similar properties to constitute a region. Specifically, one seed pixel is found to be a growing point of the growing region and then combined with the same or similar properties of the seed pixels in the neighborhood of the seed pixels into the region where the seed pixels are located. These new pixels as new seed pixels continue the above process until the pixels that are not satisfied can be included. Such a zone is growing. The core of the threshold segmentation method is how to find an appropriate threshold. The most commonly used threshold method is based on the method of gray histogram, such as the maximum interclass equation method (OTSU), minimum error method, maximum entropy method, and the like. Such methods typically use a fixed global threshold for the entire image. If there is a shadow or brightness distribution in the image, the segmentation effect will be affected. Different thresholds are employed in different regions of the image based on local thresholds, which have a better segmentation effect relative to the global threshold method, which is also referred to as an adaptive threshold method. The selection of the threshold is generally based on the local statistical information, such as local variance, partial contrast, and surface fitting threshold. Whether it is a global threshold or a partial threshold, the threshold method is usually affected by noise. In order to obtain better segmentation results, it is often also necessary to combine with other image processing techniques such as image denoising. The advantage of threshold segmentation is that the calculation is simple, the operation is high, and the speed is fast. The selection of the threshold needs to be determined according to the specific problem, generally determined by experiments. For a given image, the optimal threshold can be determined by analyzing the method of the histogram, such that when the histogram is clearly present, two peak midpoints can be selected as the optimal threshold, as shown in Figure 4.

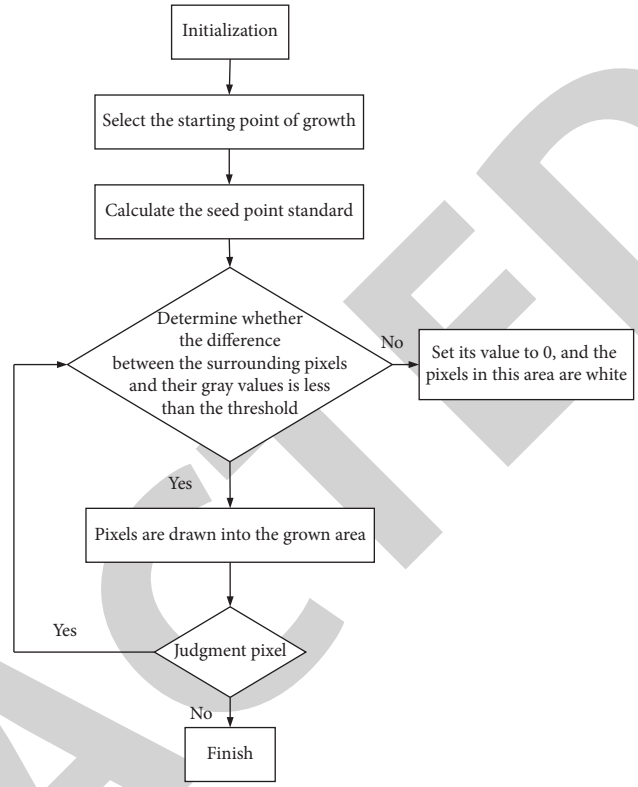

Figure 4: Segmentation flowchart based on the threshold region growing algorithm.

3. Experimental Results of Common Acute Abdominal Diseases in General Surgery Based on CT Images

3.1. Treatment of the Acute Abdomen under the ERAS Concept. Enhanced recovery after surgery (ERAS) refers to the implementation of various proven methods in the perioperative period to reduce the stress and complications of surgical patients. Reduce physical and psychological trauma and stress, reduce fatality rate and shorten hospital stay, and speed up the recovery of patients. Since its introduction, the ERAS concept has been used in various elective surgeries, such as upper gastrointestinal perforation, acute cholecystitis, and acute appendicitis [29]. Many studies have been reported on the use of the ERAS concept in the perioperative period of clinical surgical emergencies requiring emergency surgery, and the research results have shown that the application of the ERAS concept in the perioperative period of emergency abdominal diseases can achieve good clinical results corresponding to those in elective surgery, and the results of these studies have shown that the application of the ERAS concept to the perioperative period of acute abdomen can achieve good clinical outcomes in elective surgery and create a new model of perioperative management in clinical surgery. Acute abdomen is characterized by rapid onset, rapid changes, complex causes, and heavy morbidity, and the stressful stimuli caused by the onset and perioperative period are more severe than those caused by elective laparoscopic lesions, so the ERAS concept is urgently needed. In this study, we attempted to explore the importance of perioperative nutritional support therapy in the diagnosis of acute abdomen under the ERAS concept.

The case selected in this study was collected in hospitalization in a rehabilitation area of a hospital, and thirty patients with patients in income national standards. According to the order before and after admission, follow

the proportion of 1 : 1 and follow the simple digital table to randomly divide the treatment group and control group, 15 cases. All kinds of diseases are divided into two groups according to simple randomization, namely, ERAS group and CPM group. Among them, the acute abdomen cases in parallel emergency treatment have been selected as an object, mainly involving acute appendicitis, acute gallbladder inflammation, acute intestinal obstruction, upper digestive pipe perforation, and acute pancreatitis. And they are classified here.

There was no statistically significant difference in the composition of patients between the ERAS group and the CPM group, and the differences in age, gender, nutritional status before surgery, and surgical methods between the two groups were not statistically significant. Figure 5 shows the composition of the two groups of patients, and Figure 6 shows the comparison of the general conditions of the two groups of patients admitted to the hospital. Among them, A means acute appendicitis, B means acute cholecystitis, C means acute intestinal obstruction, D means gastrointestinal perforation, and E means acute pancreatitis.

Intraoperative nutrient metabolism is mainly based on restrictive infusion and regulation of blood glucose, while the patient is under intraoperative anesthesia with intraperitoneal injection, but because the organism remains in a state of stress, the surgery also causes an inductive stimulation of the organism, resulting in increased catabolism. Under stressful conditions, the human organism produces sympathetic excitation and launches various management systems including renin-angiotensin-aldosterone system and hypothalamic-pituitary hormone, etc., while many active hormones in the above management systems, such as aldosterone and antidiuretic hormone, also have a great impact on the balance of fluids in the body. Table 1 shows the comparison of NRS2002 scores between the two groups of patients. Through statistical treatment, acute appendicitis, acute gallbladders, acute intestinal obstruction, digestive tract perforation, and acute pancreatitis P values are greater than 0.05, and there is no significant difference.

In the general preoperative period, the proposed patient may not take in enough fluid or lose too much due to loss of appetite, fasting, diarrhea, nausea, etc. This results in a large loss of body fluids and insufficient effective circulating blood volume, while the traditional rehydration is the sum of the preoperative loss, the required amount, and the intraoperative and postoperative loss. The large amount of rehydration increases the effective circulatory load of patients, which can lead to gastrointestinal vascular edema, heart failure, pulmonary edema, etc., and the increase of overload effective circulation causes the oversaturation of bacterial and extrabacterial fluids, and the physiological function is constrained to a certain extent, which directly affects the postoperative wound healing, and when aggravated, it can also cause intestinal mucosal edema and prevent the normal repair of intestinal functions and even cause postoperative complications. Therefore, the rehydration method should be controlled to prevent unnecessary postoperative complications caused by excessive burden of systemic fluid and promote the recovery of the body after surgery. The theory of ERAS suggests the use of epidural anesthesia, which inhibits parasympathetic stimulation signaling and thus reduces the release of stress-related hormones, which has a favorable negative impact on glucose metabolism disorders and multiple fluid homeostasis. The dose of glucose injected during surgery should also be appropriately controlled, and the phenomenon of insulin resistance in the postoperative period should be reduced. Table 2 compares the surgical methods of the two groups of patients.

3.2. Treatment of the Acute Abdomen by ERAS Based on CT Images. Compared with the CPM group, the duration of postoperative recovery of colorectal function was significantly reduced in the ERAS group, and this difference was more statistically significant ($P < 0.05$). Compared with the CPM group, the ERAS group had earlier time to first bed activity and first meal and also had lower postoperative pain level, and this difference was more statistically significant ($P < 0.05$). Figure 7 shows the comparison of the relevant indexes of the two groups of acute appendicitis patients after the operation of acute cholecystitis patients. The nutritional method for acute abdomen surgery under the ERAS concept is water intake for six hours after the operation; liquid food is gradually started on the first day after the operation and then slowly added every day according to the patient's tolerance until the full dose.

How to provide proper nutritional protection after surgery depends on the nutritional status before surgery and the gastrointestinal function status after surgery. ERAS advocates early postoperative diet, and early feeding stimulation can shorten the duration of gastrointestinal ischemia, thereby reducing the reperfusion injury to the gastrointestinal mucosa and improving the peristalsis of the large intestine, thereby promoting the repair of intestinal function. Under normal circumstances, supine patients need to be given about 20–25 kcal of heat energy per kilogram weight per day, but if the patient is still able to move independently, it needs to increase the energy consumption of about 5 kcal/(kg d). The transition of nutrient sources from intestinal nutrition to conventional diet cannot be accomplished overnight and must be gradually improved with the patient's tolerance status. Usually, one-fourth of the full dose can be given on the first day, but the nutrients must fully meet the patient's needs for healing and recovery; one-half of the full dose can be given after the second day, and the full dose of enteral nutrition can be given after the third day if circumstances permit. For patients who cannot receive enteral nutrition in a short period of time, they can choose to combine enteral nutrition with parenteral nutrition. As shown in Figure 8, it is a comparison of the indicators of the two groups of patients with acute intestinal obstruction after surgery and those with gastrointestinal perforation, where a represents the date of intestinal function returning to normal, b represents the date of first getting out of bed, and c represents the time of first eating. Figure 9 is a picture of a patient with complete intestinal obstruction observed on the basis of CT images. The left picture in Figure 10 shows a perforation of the digestive tract observed on the basis of CT

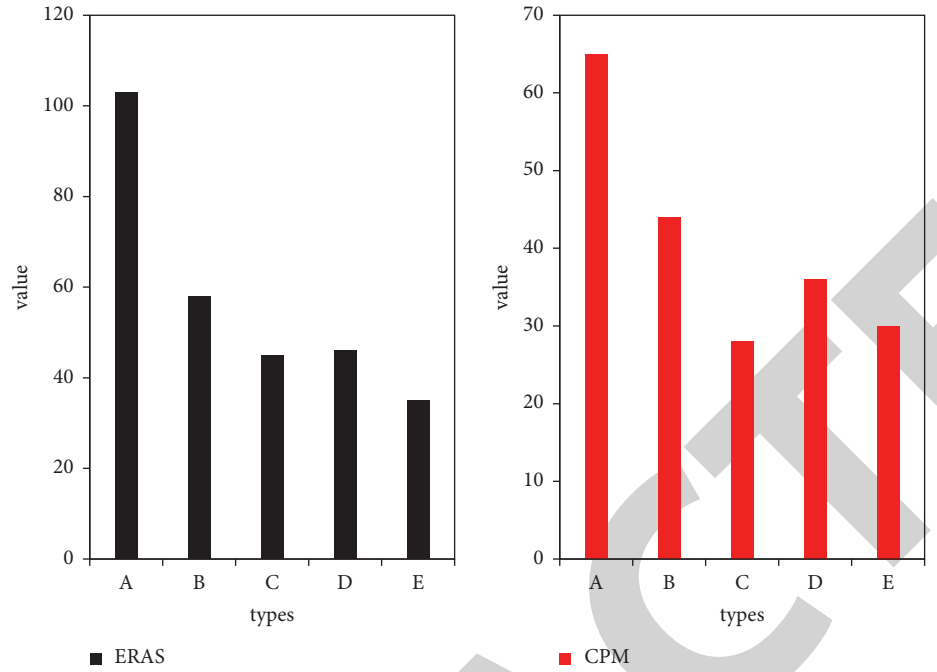

Figure 5: Disease composition of the two groups of patients/case.

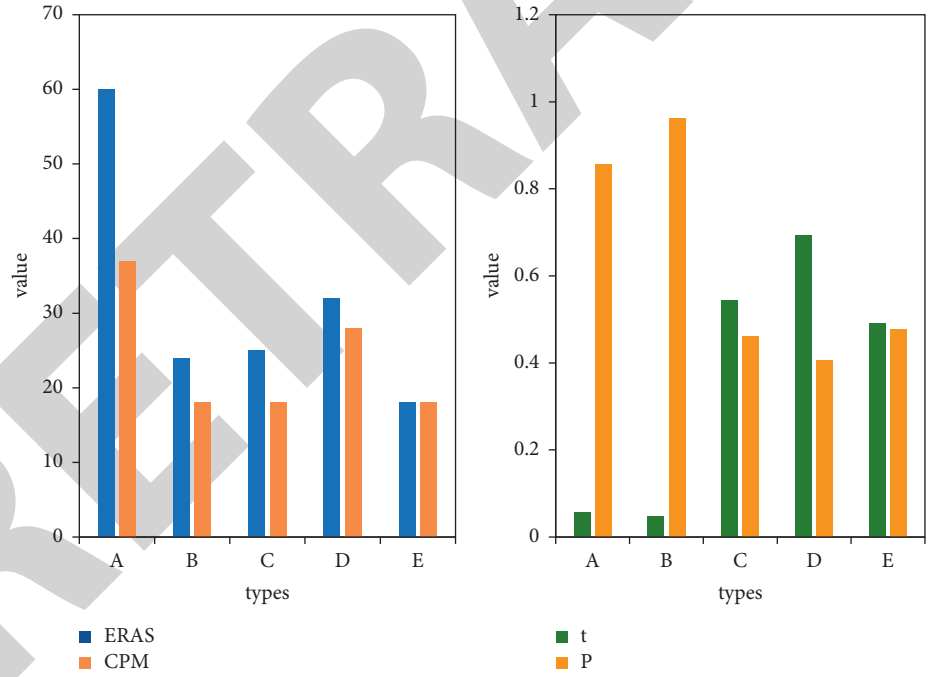

Figure 6: Comparison of the general conditions of the two groups of patients admitted to the hospital/case.

Table 1: Comparison of NRS2002 score between two groups of patients/case.

Group	Acute appendicitis		Acute cholecystitis		Acute intestinal obstruction		Digestive tract perforation		Acute pancreatitis	
	>3	<3	>3	<3	>3	<3	>3	<3	>3	<3
ERAS	19	79	9	36	19	24	26	20	14	19
CPM	13	49	8	47	9	15	14	19	15	17
T	0.319		0.169		0.249		1.298		0.597	
P	0.571		0.678		0.609		0.249		0.441	

Table 2: Comparison of surgical methods between the two groups of patients/case.

Group	Acute appendicitis		Acute cholecystitis		Acute intestinal obstruction		Digestive tract perforation		Acute pancreatitis
	Simple appendectomy	Appendectomy + abscess removal	Cholecystectomy	Cholecystectomy + bile duct exploration	Bowel arrangement	Bowel resection and anastomosis	Perforation repair	Bowel resection and anastomosis	Abdominal abscess removal
ERAS	90	13	23	33	21	24	29	20	36
CPM	49	11	19	22	12	10	23	9	29
T	0.691		0.411		0.149		0.988		-
P	0.401		0.519		0.701		0.309		-

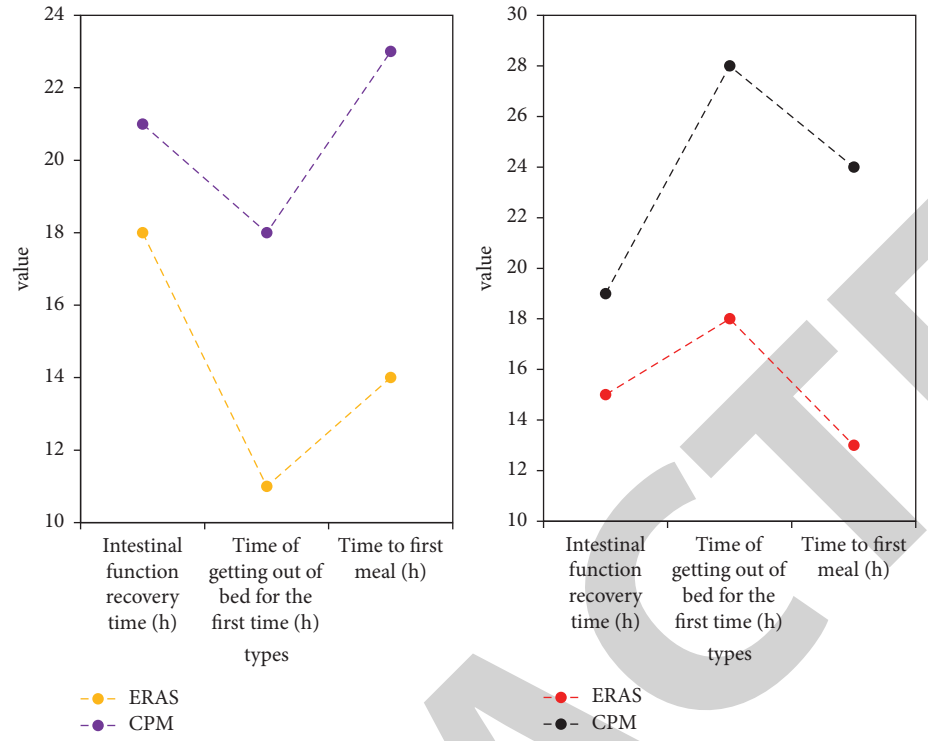

Figure 7: Comparison of related indexes of (a) two groups of patients with acute appendicitis after surgery and (b) two groups of patients with acute cholecystitis.

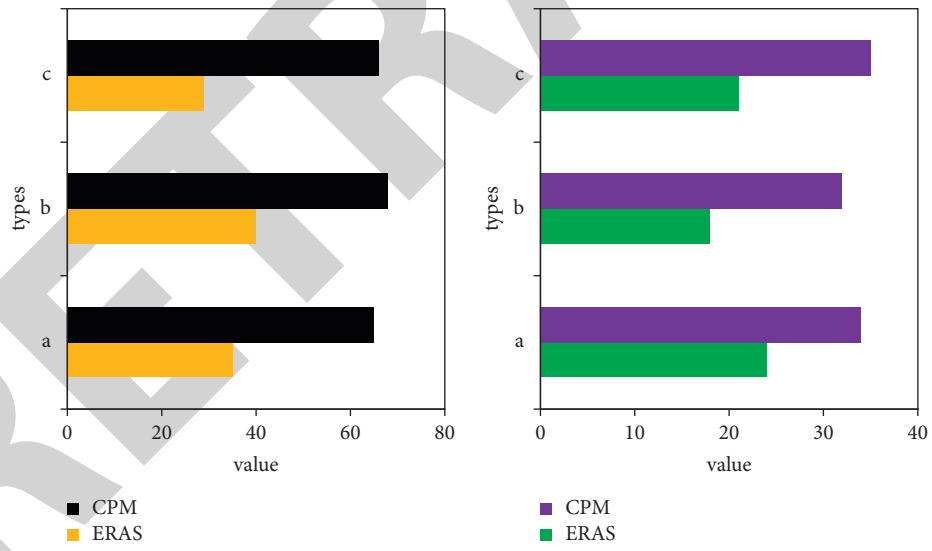

Figure 8: Comparison of related indexes between (a) the two groups of patients with acute intestinal obstruction after surgery and (b) the two groups of patients with gastrointestinal perforation.

images, and the right picture shows a normal abdominal radiograph observed on CT images.

Postoperative pain can prolong the patient's bed rest or delay the return of bowel function to normal, but not every pain medication is suitable for perioperative application; for example, opioid analgesics can reduce intestinal peristalsis and increase the risk of postoperative intestinal obstruction, which can prolong the time to the first meal; ERAS emphasizes epidural pain pump + administration of NSAIDs, while reducing opioid analgesics for multimodel pain treatment can somewhat reduce this adverse effect. Table 3 shows the comparison of the relevant indexes of the two groups of patients with acute pancreatitis after operation.

Table 4 compares the clinical outcomes of the two groups of patients. ERAS combined with some optimization initiatives in the perioperative period can increase the possibility of early postoperative transdigestive nutrition, such as nonroutine preoperative cleaning of the gastrointestinal

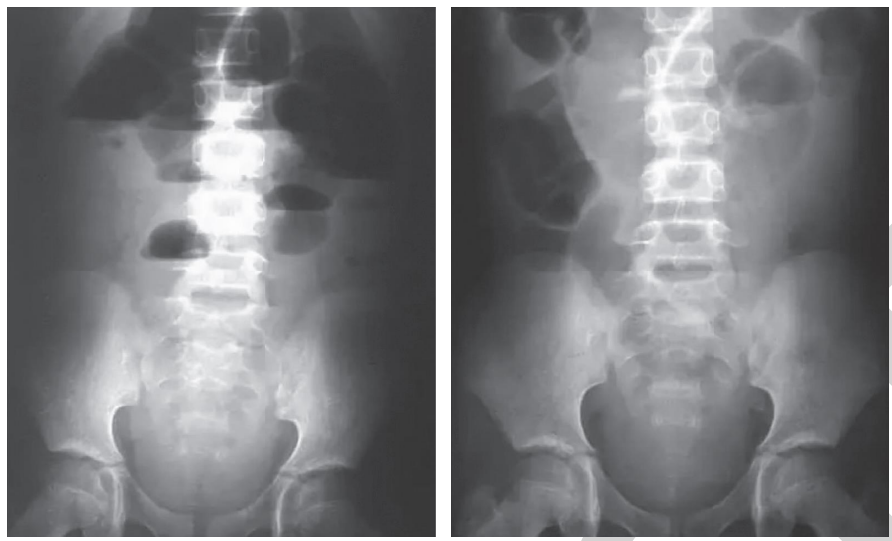

Figure 9: Complete intestinal obstruction.

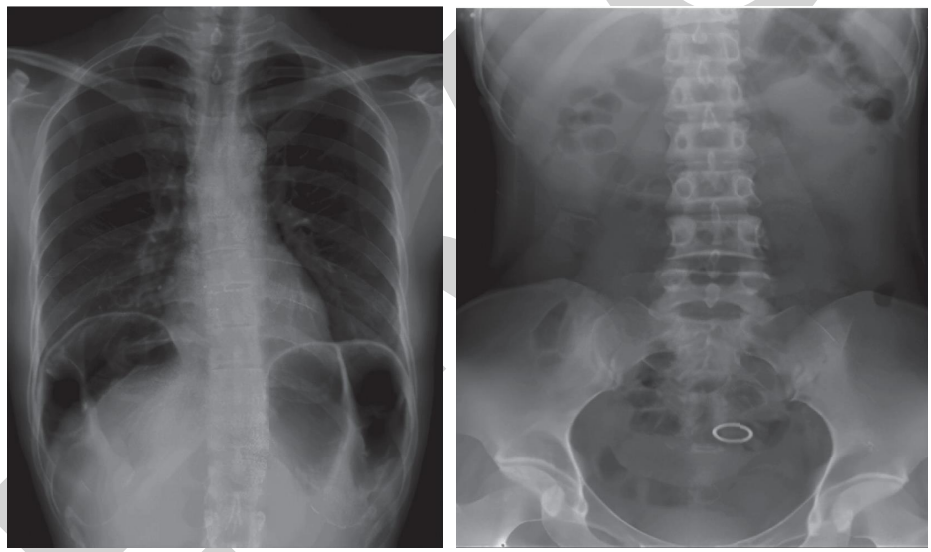

Figure 10: (a) Perforation of the digestive tract; (b) a normal abdominal slice.

Table 3: Comparison of related indexes of two groups of patients with acute pancreatitis after operation.

Group	Intestinal function recovery time (h)	Time of getting out of bed for the first time (h)	Time to first meal (h)
ERAS	35	31	33
CPM	47	37	49
T	5.98	3.387	7.821
P	<0.001	0.001	<0.001

Table 4: Comparison of clinical results between the two groups of patients.

Group	Postoperative complications/case (%)	Postoperative hospital stay (d)
ERAS	18	5.34
CPM	26	9.07
T	8.012	19.987
P	0.05	<0.001

tract, early postoperative removal of nasogastric and urinary catheters, restrictive rehydration, epidural anesthesia and less damaging surgical methods, early postoperative activity, and multimodal postoperative analgesia, reducing stressful stimuli caused by disease and the postoperative environment, thus minimizing the impact on the nutritional and metabolic systems. This reduces the incidence of postoperative comorbidities, shortens the duration of postoperative hospitalization, reduces medical expenses, and promotes the ultimate goal of recovery. The ERAS concept has outstanding advantages for lower perioperative nutritional support and comparison with conventional perioperative management, as ERAS offers benefits to patients by shortening the postoperative hospitalization time frame.

4. Discussion

The main objective of nutritional support in combination with other perioperative optimization measures is to reduce the stressful stimulation of the patient, thus reducing the postoperative disruption of nutrition and metabolism, reducing the incidence of postoperative comorbidities, reducing the length of hospital stay, and reducing medical expenses, in order to achieve the goal of accelerated recovery of the patient. The results of this investigation showed that perioperative nutritional support under the concept of ERAS had outstanding advantages compared with traditional perioperative management methods, and the postoperative complication rate in the ERAS group was only 6.01% compared with 12.9% in the traditional CPM group, which was a statistically significant improvement ($P < 0.05$). The postoperative hospital stay was also reduced from 7.93 days to 4.62 days, thus controlling the clinical risk during the perioperative period and bringing benefits to patients. Compared with the CPM group, the rapid recovery of gastrointestinal function and the first meal in the ERAS group after surgery were significantly earlier than those in the CPM group. This was achieved through a combination of enhanced communication with patients and families before surgery to obtain full cooperation, nonroutine placement of nasogastric tubes, epidural intraperitoneal infusion anesthesia treatment and analgesia, small postoperative incisions, control of the amount of vomiting and diarrhea, reduction of opioid analgesics within perioperative resourcefulness, and the results of a series of measures such as early postoperative bedtime activities.

5. Conclusions

In the postoperative treatment of acute abdominal disease, we advocate individualized treatment, specific solutions for various conditions of patients, and carefully grasp the nutrient requirements of patients, metabolic function, and nutrient giving pathways and effects, so that we can achieve the desired goal of postoperative nutritional support care for acute abdominal disease. In the case of patients with acute abdomen, nutritional support under the ERAS concept has made it possible to provide patients with shorter hospital stays, significantly improved organ function, significantly improved nutrient status, and increased comfort, and there is no increase in the number of patients, with good publicity and promotion, thus providing the greatest possible benefit to patients. The standardized and reasonable management of nutritional support in the peripheral period can enhance the immune function, adjust metabolism, maintain tissue and organ function and control inflammatory response, and thus improve the outcome of surgical care, which is the development direction that must be pursued by surgical nutrient caregivers in the future. In patients with acute abdomen undergoing emergency surgery, the use of perioperative nutrient support measures under the theory of accelerated repair surgery can effectively improve the nutritional status of patients, accelerate postoperative recovery, and reduce surgical complications, thereby reducing the length of hospitalization and optimizing clinical outcomes. The core of accelerating the surgery of rehabilitation is to reduce surrounding wound stress and promote rapid recovery of each organ function. Perioperative wound stress response is the earliest effect on gastrointestinal function, but the last one continues. Perioperative treatment measures have different degrees of gastrointestinal function recovery after surgery, and improper treatment will result in postoperative gastrointestinal function recovery delays. In this regard, we will further study.

Data Availability

The data that support the findings of this study are available from the corresponding author upon reasonable request.

Disclosure

Yunguang Nan and Zuyan Zhang are the co-first authors.

Conflicts of Interest

The authors declare that they have no conflicts of interest.

Authors' Contributions

Yunguang Nan and Zuyan Zhang authors contributed equally to this work.

References

[1] S. Zhang, F. Sun, N. Wang et al., "Computer-aided diagnosis (CAD) of pulmonary nodule of thoracic CT image using transfer learning," *Journal of Digital Imaging*, vol. 32, no. 6, pp. 995–1007, 2019.

[2] Y. Li and L. Xia, "Coronavirus disease 2019 (COVID-19): role of chest CT in diagnosis and management," *AJR. American journal of roentgenology*, vol. 214, no. 6, pp. 1280–1286, 2020.

[3] M. Metintas, H. Yildirim, T. Kaya et al., "CT scan-guided Abrams' needle pleural biopsy versus ultrasound-assisted cutting needle pleural biopsy for diagnosis in patients with pleural effusion: a randomized, controlled trial," *Respiration*, vol. 91, no. 2, pp. 156–163, 2016.

[4] E. R. Ropelle, M. B. Flores, D. E. Cintra et al., "IL-6 and IL-10 anti-inflammatory activity links exercise to hypothalamic

insulin and leptin sensitivity through IKKβ and ER stress inhibition," *PLoS Biology*, vol. 8, no. 8, pp. 697–704, 2019.

[5] K. G. Srinivasa K G, B. J. Sowmya Bj, A. Shikhar, R. Utkarsha, and A. Singh, "Data Analytics assisted internet of things towards building intelligent healthcare monitoring systems," *Journal of Organizational and End User Computing*, vol. 30, no. 4, pp. 83–103, 2018.

[6] L. V. van Dijk, C. L. Brouwer, A. van der Schaaf et al., "CT image biomarkers to improve patient-specific prediction of radiation-induced xerostomia and sticky saliva," *Radiotherapy and Oncology*, vol. 122, no. 2, pp. 185–191, 2017.

[7] Z. Dong, H. Jing, Z. Hua et al., "Spectral CT image restoration via an average image-induced nonlocal means filter," *IEEE Transactions on Biomedical Engineering*, vol. 63, no. 5, pp. 1044–1057, 2016.

[8] Z. Hao, H. Hao, Z. Liang et al., "Extracting information from previous full-dose CT scan for knowledge-based bayesian reconstruction of current low-dose CT images," *IEEE Transactions on Medical Imaging*, vol. 35, no. 3, pp. 860–870, 2016.

[9] P. Shan and X. Lai, "Influence of CT scanning parameters on rock and soil images," *Journal of Visual Communication and Image Representation*, vol. 58, no. 1, pp. 642–650, 2019.

[10] C. Helma, T. Cramer, S. Kramer et al., "Data mining and machine learning techniques for the identification of mutagenicity inducing substructures and structure activity relationships of noncongeneric compounds," *J Chem Inf Comput*, vol. 35, no. 4, pp. 1402–1411, 2018.

[11] M. P. Hosseini, H. Soltanian-Zadeh, and S. Akhlaghpoor, "Computerized processing and analysis of CT images for developing a new criterion in COPD diagnosis," *The Journal of the Geological Society of Japan*, vol. 29, no. 174, pp. 643–657, 2016.

[12] Y. Herrera-Martínez, J. J. Martín-Marcuartu, J. Mohigefer Barrera, J. M. Jiménez-Hoyuela, and R. García Jiménez, "Hybrid image (SPECT/CT) in the early diagnosis of a patient with calciphylaxis - ScienceDirect," *Nefrologia*, vol. 40, no. 5, pp. 576–578, 2020.

[13] M. C. Christensen, C. Dreier, and J. Becher, "Diagnosis of pulmonary Artery embolism: comparison of single-source CT and 3rd generation dual-source CT using a dual-energy protocol regarding image quality and radiation dose," *Röfo*, vol. 189, no. 06, pp. 527–536, 2017.

[14] A. Varga-Szemes, J. L. Wichmann, U. J. Schoepf et al., "Accuracy of n quiescent-interval single-shot lower extremity MR Angiography versus CT Angiography for diagnosis of peripheral Artery disease," *JACC: Cardiovascular Imaging*, vol. 10, no. 10, pp. 1116–1124, 2017.

[15] R. KonstantinovskyD. Cohen et al., "Comparing effective doses during image-guided core needle biopsies with computed tomography versus C-Arm cone beam CT using Adult and pediatric phantoms," *Cardiovascular and Interventional Radiology: A Journal of Imaging in Diagnosis and Treatment*, vol. 39, no. 5, pp. 732–739, 2016.

[16] S. Byott and I. Harris, "Rapid acquisition axial and coronal T2 HASTE MR in the evaluation of acute abdominal pain," *European Journal of Radiology*, vol. 85, no. 1, pp. 286–290, 2016.

[17] S. R. Best, L. E. Romine, and M. A. Brown, "Magnetic resonance imaging of acute abdominal and pelvic pain in pregnancy," *Topics in Magnetic Resonance Imaging*, vol. 23, no. 4, pp. 225–242, 2016.

[18] P. M. García, L. F. López-Jurado, and A. V. Bártulos, "Acute abdominal pain in patients with Crohn's disease: what urgent imaging tests should be done?" *Radiología (English Edition)*, vol. 61, no. 4, pp. 333–336, 2019.

[19] C. Kiyoshi, K. Shota, S. Hirotoshi, S. Yuka, and O. Hirokuni, "Complicated Acute Neurological Beh?et's Disease after Surgical Repair of Abdominal Artery Aneurysms," *Japanese Journal of Vascular Surgery*, vol. 28, no. 1, pp. 53–56, 2019.

[20] A. Jamal Talabani, B. H. Endreseth, S. Lydersen, and T.-H. Edna, "Clinical diagnostic accuracy of acute colonic diverticulitis in patients admitted with acute abdominal pain, a receiver operating characteristic curve analysis," *International Journal of Colorectal Disease*, vol. 32, no. 1, pp. 41–47, 2016.

[21] A. Rezaei, C. Michel, M. E. Casey, and J. Nuyts, "Simultaneous reconstruction of the activity image and registration of the CT image in TOF-PET," *Physics in Medicine and Biology*, vol. 61, no. 4, pp. 1852–1874, 2016.

[22] M. P. Wenzl, M. Heller, V. Janz, C Perka, and G. I Wassilew, "Validation of CT image-based software for three-dimensional measurement of acetabular coverage profile," *Technology and Health Care: Official Journal of the European Society for Engineering and Medicine*, vol. 25, no. 6, pp. 989–1004, 2017.

[23] S. Echegaray, V. Nair, M. Kadoch et al., "A rapid segmentation-insensitive "digital biopsy" method for r feature extraction: method and pilot study using CT images of non-small cell lung cancer," *Tomography*, vol. 2, no. 4, pp. 283–294, 2016.

[24] M. Hu, Y Zhong, S. Xie, H. Lv, and Z. Lv, "Fuzzy system based medical image processing for brain disease prediction," *Frontiers in Neuroscience*, vol. 15, p. 965, 2021.

[25] S. Han, K. Choi, S. W. Yoo, and J. Yi, "A distance-driven deconvolution method for CT image-resolution improvement," *Journal of the Korean Physical Society*, vol. 69, no. 12, pp. 1830–1833, 2016.

[26] J. Bian, G. C. Sharp, Y.-K. Park, J. Ouyang, T. Bortfeld, and G. El Fakhri, "Investigation of cone-beam CT image quality trade-off for image-guided radiation therapy," *Physics in Medicine and Biology*, vol. 61, no. 9, pp. 3317–3346, 2016.

[27] Y. Sun, L. Zhang, T. Fei, and X. Liu, "Variational Bayesian blind restoration reconstruction based on shear wave transform for low-dose medical CT image," *EURASIP Journal on Image and Video Processing*, vol. 2017, no. 1, pp. 1–10, 2017.

[28] H. S. Nguyen, M. Patel, L. Li, S. Kurpad, and W. Mueller, "Quantitative estimation of a ratio of intracranial cerebrospinal fluid volume to brain volume based on segmentation of CT images in patients with extra-axial hematoma," *The Neuroradiology Journal*, vol. 30, no. 1, pp. 10–14, 2017.

[29] S. K. Gupta, S. Trethewey, B. Brooker et al., "Radionuclide bone scan SPECT-CT: lowering the dose of CT significantly reduces radiation dose without impacting CT image quality," *American Journal of Nuclear Medicine and Molecular Imaging*, vol. 7, no. 2, pp. 63–73, 2017.